Bistatic Architecture Provides Extended Coverage and System Reliability in Scatter Sensor Networks

Konstantinos Tountas*, Panos N. Alevizos*, Aikaterini Tzedaki† and Aggelos Bletsas*
*School of ECE, Technical Univ. of Crete, Greece, {ktountas, palevizos}@isc.tuc.gr, aggelos@telecom.tuc.gr
†School. of PEM, Technical Univ. of Crete, Greece, katerina.tzed@gmail.com

***Abstract*—Scatter radio is a promising enabling technology for ultra-low power consumption and low monetary cost, large-scale wireless sensor networks. The two most prominent scatter radio architectures, namely the *monostatic* and the *bistatic*, are compared. Comparison metrics include bit error probability under maximum-likelihood detection for the single-user case and outage probability for the multi-user case (including tight bounds). This work concretely shows that the bistatic architecture improves coverage and system reliability. Utilizing this fact, a bistatic, *digital* scatter radio sensor network, perhaps the first of its kind, using frequency-shift keying (FSK) modulation and access, is implemented and demonstrated.**

I. Introduction

Scatter radio, i.e., communication by means of reflection rather than radiation [1], utilizes a single radio frequency (RF) transistor, in contrast to conventional Marconi radios that require energy-consuming mixers and amplifiers, signal conditioning units and complex RF front-ends. The most prominent use of scatter radio is in radio frequency identification (RFID), widely used for inventorying, electronic tickets, people identification [2] or even musical instruments [3], [4]. Current industry standards (such as UHF EPC Class 1, Generation 2 [5]) focus on the aforementioned applications, disregarding the value of scatter radio in wireless sensor networks (WSNs); the simplicity of the front-end minimizes the energy and monetary cost of each sensor node. Proof of concept systems utilizing scatter radio in WSNs have been presented in [6]–[10].

Typical RFID systems utilize passive tags and monostatic architecture to operate. Passive tags typically employ energy harvesting to power their electronics and relatively high bit rate, resulting to short range; a monostatic architecture is typically utilized with the reader including both the transmitter of the carrier wave (CW) needed for tag operation and the receiver, responsible for tag information reception. In order to increase network coverage, recent work has proposed semi-passive tags (i.e., energy assisted) and low bit rate [6], as well as bistatic architecture with non-coherent [10] or coherent [11] processing, even with exploitation of short block-length channel codes [12], [11], [13]. In the bistatic architecture the reader and the carrier emitter are not co-located. Thus, more flexible topologies can be set up.

However, prior art has not investigated which architecture is more suitable for increasing coverage and reliability of scatter sensor *networks*. Link budgets for monostatic and bistatic links were studied in [14]. Additionally, authors in [15] investigated the link-envelope correlation of the dyadic backscatter channel (i.e., the most general backscatter channel), concluding that the use of separate transmitter and receiver antennas can reduce the point-to-point bit-error-rate (BER). Moreover, work in [16] offered closed formed expressions for the outage probability of monostatic scatter sensor networks. An analog bistatic scatter radio WSN was presented in [17].

This work offers analysis of the monostatic and the bistatic architectures for scatter WSNs. The two architectures are compared in terms of BER under maximum-likelihood (ML) FSK detection for single user communication [11], as well as probability of outage for multi-user communication. In the latter case, tight Jensen-based upper bounds are derived. It is shown that the bistatic architecture increases both coverage and system reliability. Utilizing the bistatic architecture, a proof-of-concept prototype digital scatter WSN is demonstrated; it consists of semi-passive tags employing FSK modulation and frequency division multiplexing (FDM), allowing simultaneous, collision-free operation of multiple sensors-tags. Practical difficulties in crafting such digital scatter radio network are discussed. This work complements [10], where digital, single-tag operation was demonstrated in a bistatic setup.

The rest of this work is organized as follows. Section II presents the channel models of both monostatic and bistatic architectures. Section III presents the single user (i.e. tag) error probability analysis, and Section IV offers the outage probability analysis for multiple users. Numerical results are presented in Section V. Section VI presents a prototype, digital bistatic scatter radio sensor network, perhaps the first of its kind. Finally, Section VII concludes the paper.

II. Scatter Radio Architecture Analysis

A. Backscatter Wireless Propagation Channel

A scatter radio WSN is considered of N tags that transmit their measured data to a software-defined radio (SDR) reader; the set of all tags is denoted as $U \triangleq \{1, \cdots, N\}$.

In the monostatic architecture the reader functions as both the receiver and the CW emitter; the reader transmits the CW, illuminating the tags, which modulate their information on the incident signal and reflect the modulated signal back to the SDR reader. Thus, N bidirectional links exist (i.e. between the reader and the N tags), as shown in Fig. 1-Left. The distance between the reader and the n-th tag is denoted by d_{k}^{n}, where $\mathrm{k} \in \{\mathrm{TR}, \mathrm{RT}\}$ denotes the direction of the link (tag-to-reader

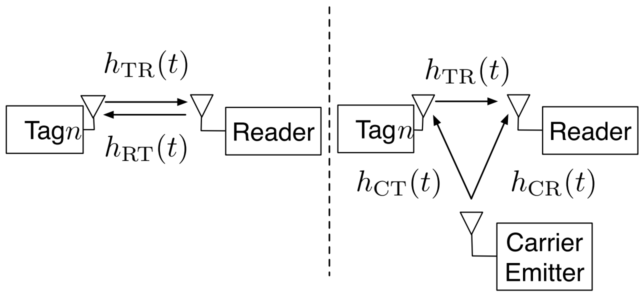

Fig. 1. Left: Monostatic channel model. Right: Bistatic channel model.

or reader-to-tag, respectively) and $n \in U$ is the index of n-th tag.

In the bistatic architecture the carrier emitter and the receiver are not co-located. The emitter is a separate device placed away from the reader, as shown in Fig. 1-Right. In this case there are $2N$ unidirectional links (N carrier emitter-to-tag links and N tag-to-reader links) plus the carrier emitter-to-reader link. The distance between the carrier emitter and the n-th tag is denoted by d^n_{CT}, while the distance between the n-th tag and the reader is denoted as d^n_{TR} with $n \in U$.

Both system architectures experience path loss and small-scale fading. Taking into account the line-of-sight (LOS) path between the receive and the transmit antennas, as well as the reflection from the ground (two-ray model), the one-way path loss can be approximated by [6]:

$$L^n_{\mathrm{k}} = \begin{cases} G_{\mathrm{Tx(k)}} G_{\mathrm{Rx(k)}} \left(\frac{\lambda}{4\pi d^n_{\mathrm{k}}}\right)^2, & \text{if } d^n_{\mathrm{k}} < d_0(\mathrm{k}) \\ G_{\mathrm{Tx(k)}} G_{\mathrm{Rx(k)}} \left(\frac{\mathsf{h}_{\mathrm{Tx(k)}} \mathsf{h}_{\mathrm{Rx(k)}}}{(d^n_{\mathrm{k}})^2}\right)^2, & \text{if } d^n_{\mathrm{k}} \geq d_0(\mathrm{k}), \end{cases} \tag{1}$$

with $\mathrm{Tx(k)}$ and $\mathrm{Rx(k)}$ denoting the transmitter and receiver of link k, where $\mathrm{k} \in \{\mathrm{CT}, \mathrm{TR}\}$ or $\mathrm{k} \in \{\mathrm{RT}, \mathrm{TR}\}$ for bistatic and monostatic topologies, respectively and $d_0(\mathrm{k})$ is given by:

$$d_0(\mathrm{k}) = \frac{4\pi \mathsf{h}_{\mathrm{Tx(k)}} \mathsf{h}_{\mathrm{Rx(k)}}}{\lambda}, \tag{2}$$

where $\mathsf{h}_{\mathrm{Tx(k)}}$ and $\mathsf{h}_{\mathrm{Rx(k)}}$ are the heights of the transmitter and the receiver, respectively and λ denotes the wavelength. Note that for the monostatic topology $d^n_{\mathrm{TR}} = d^n_{\mathrm{RT}}$, due to the reciprocal nature of the channel.

Frequency non-selective (flat fading) channels are assumed, since the communication bandwidth and the delay spread are relatively small. The complex baseband channel impulse response of each link is depicted in Fig. 1-Left and Right for monostatic and bistatic topologies, respectively. Channel coherence time is denoted as T_{coh} and the complex channel gains are are given by:

$$h^n_{\mathrm{k}}(t) = h^n_{\mathrm{k}} = a^n_{\mathrm{k}}\, e^{-j\phi^n_{\mathrm{k}}}, \tag{3}$$

where $\mathrm{k} \in \{\mathrm{CT}, \mathrm{TR}\}$ or $\mathrm{k} \in \{\mathrm{RT}, \mathrm{TR}\}$ for bistatic and monostatic topologies, respectively. $a^n_{\mathrm{k}} \in \mathbb{R}_+$ denotes the channel attenuation parameter and $\phi^n_{\mathrm{k}} \in [0, 2\pi)$ denotes the phase shift introduced by the propagation delay. The channel impulse response parameters change independently every T_{coh}. The probability density function (PDF) of the channel amplitude, $a^n_{\mathrm{k}} = |h^n_{\mathrm{k}}|$, $\mathrm{k} \in \{\mathrm{CT}, \mathrm{TR}\}$ or $\mathrm{k} \in \{\mathrm{RT}, \mathrm{TR}\}$, is assumed Rayleigh:

$$f_{|h^n_{\mathrm{k}}|}(x) = \frac{2x}{\sigma^2_{\mathrm{k}}} e^{-\frac{x^2}{\sigma^2_{\mathrm{k}}}}, \quad x \geq 0. \tag{4}$$

Without loss of generality, $\sigma^2_{\mathrm{k}} = 1$.

B. Frequency Division Multiplexing (FDM) based on BFSK

The use of BFSK modulation allows the use of FDM architecture for the network, i.e., each tag n uses a unique set of subcarrier frequencies $F^n_i, i \in \mathbb{B} \triangleq \{0, 1\}$ to scatter its information. In contrast to classic FSK, the backscatter FSK modulation uses 4 frequencies, $\pm F^n_i, i \in \mathbb{B}$. Therefore, the classic FSK demodulator can not be used, since this will result to 3 dB loss in performance [10]. For each tag, under the orthogonality criterion, for noncoherent FSK two conditions must hold:

$$|F_i - F_{\mathrm{z}}| = \frac{k}{T} \quad \text{and} \quad F_i \gg \frac{1}{T}, \tag{5}$$

and for coherent FSK:

$$|F_i - F_{\mathrm{z}}| = \frac{k}{2T}, \quad \text{and} \quad F_i \gg \frac{1}{2T}, \tag{6}$$

$\forall i, \mathrm{z} \in \mathbb{B} : i \neq \mathrm{z}$, and $k \in \mathbb{N}$. From (5) and (6) it can be shown that [10]:

$$\int_T e^{j\,2\,\pi\, F_i t} \left(e^{j\,2\,\pi\, F_{\mathrm{z}} t}\right)^* dt = \begin{cases} T, & F_i = F_{\mathrm{z}}, \\ 0, & \text{otherwise,} \end{cases} \quad , \tag{7}$$

where $\mathrm{z}, i \in \mathbb{B}$ and the integration is performed over one bit period T. The set of exponentials of frequencies $\pm F_i, i \in \mathbb{B}$, normalized by $\sqrt{T}$, constitute an orthonormal basis that can be used for expansion of the received signal. The system is converted to N parallel channels, resulting to single tag detection techniques used on each user. Such detection techniques have been extensively covered in [10], [11], [13]. The receiver suffers also from band-limited, circularly symmetric, complex Gaussian noise with power spectral density (PSD):

$$S_{ww}(F) = \begin{cases} \mathcal{N}_0, & |F| \leq W, \\ 0, & \text{otherwise.} \end{cases} \tag{8}$$

C. Bistatic System Model

In the bistatic architecture the carrier emitter and the reader are not co-located, as shown in Fig. 1-Right. The average received power of the n-th user at the reader is defined as:

$$P^n \triangleq \eta^n L^n_{\mathrm{CT}} L^n_{\mathrm{TR}} P_{\mathrm{C}}, \quad n \in U, \tag{9}$$

where $L^n_{\mathrm{k}}, \mathrm{k} \in \{\mathrm{CT, TR}\}$, is the path loss, P_{C} is the power of emitter's carrier signal and η^n accounts for the scattering efficiency of the tag's antenna front-end, depending on each tag's microwave parameters. The tag's signal is affected by the compound channel:

$$h^n = h^n_{\mathrm{CT}} h^n_{\mathrm{TR}}, \quad n \in U. \tag{10}$$

It has been shown that for bistatic architecture [10], [13], the received baseband signal of the n-th user, over bit period T, with $F_i + \frac{20}{T} \ll W$ is given by:

$$\mathbf{r}^n = h^n\, \mathbf{x}_i^n + \mathbf{w}^n, \quad n \in U, \tag{11}$$

where the vector $\mathbf{x}_i^n$ is defined as:

$$\mathbf{x}_i^n \triangleq C^n \sqrt{\frac{P^n T}{2}} \begin{bmatrix} e^{+j\Phi_0^n} \\ e^{-j\Phi_0^n} \\ e^{+j\Phi_1^n} \\ e^{-j\Phi_1^n} \end{bmatrix} \odot \mathbf{s}_i^n, \quad n \in U, \tag{12}$$

with $\mathbf{s}_i^n = [(1-i^n)\ \ (1-i^n)\ \ i^n\ \ i^n]^T$ is the four dimensional transmitted symbol of the n-th tag corresponding to bit $i^n \in \mathbb{B}$, Φ_i^n is the phase mismatch between tag n and the reader, h^n is the compound channel associated to the bistatic channel as defined in Eq. (10) and $\mathbf{w}^n \sim \mathcal{CN}(\mathbf{0}_4, \mathcal{N}_0 \mathbf{I}_4)$. Symbol $\odot$ denotes the component-wise (Hadamard) product. The parameter C^n satisfies $|C^n| = 1$ and depends on antenna related parameters of the tag n and the phase offset between the carrier emitter and the reader.

D. Monostatic System Model

Since the carrier emitter and the reader are co-located, the average received power of the n-th user at the receiver is defined as:

$$P^n \triangleq \eta^n (L_{\mathrm{k}}^n)^2 P_{\mathrm{R}}, \quad n \in U, \tag{13}$$

where P_{R} is the reader transmitted power, L_k^n is the one-way path loss, $\mathrm{k} \in \{\mathrm{RT}, \mathrm{TR}\}$.

Taking into account small-scale fading and reciprocity, $h_{\mathrm{RT}}^n = h_{\mathrm{TR}}^n$. The tag's signal is affected by the compound channel, which is the product of the two circularly symmetric complex Gaussian distributed r.vs, given by:

$$h^n = (h_{\mathrm{TR}}^n)^2, \quad n \in U. \tag{14}$$

The magnitude of h^n, $|h^n|$ is exponentially distributed, as the square of a Rayleigh random variable.

Similarly to the bistatic architecture, it can be shown that for monostatic architecture, the received baseband signal of the n-th user, over bit period T, with $F_i + \frac{20}{T} \ll W$, is given by:

$$\mathbf{r}^n = h^n\, \mathbf{x}_i^n + \mathbf{w}^n, \quad n \in U, \tag{15}$$

where the vector $\mathbf{x}_i^n$ is given in (12), h^n is the compound channel associated to the monostatic channel as defined in Eq. (14) and parameter C^n satisfies $|C^n| = 1$ and depends on the n-th tag's antenna load.

III. Probability of Error Under ML Coherent Detection

For a given channel h^n the conditional probability of error for the coherent scatter radio link is given by [18]:

$$\Pr(e \mid h^n) = Q\left(\frac{|h^n|\, \|\mathbf{x}_0^n - \mathbf{x}_1^n\|_2}{\sqrt{2\, \mathcal{N}_0}}\right), \quad n \in U, \tag{16}$$

where $\|\mathbf{x}_0^n - \mathbf{x}_1^n\|_2^2$ is given by:

$$\|\mathbf{x}_0^n - \mathbf{x}_1^n\|_2^2 = |C^n|^2\, \frac{P^n T}{2} \left\| \begin{bmatrix} e^{+j\Phi_0^n} \\ e^{-j\Phi_0^n} \\ -e^{+j\Phi_1^n} \\ -e^{-j\Phi_1^n} \end{bmatrix} \right\|_2^2 = 2P^n T. \tag{17}$$

Hence, Eq. (16) can be writen, $\forall n \in U$:

$$Q\left(\frac{|h^n|\, \|\mathbf{x}_0^n - \mathbf{x}_1^n\|_2}{\sqrt{2\, \mathcal{N}_0}}\right) = Q\left(\frac{|h^n|\ \sqrt{P^n T}}{\sqrt{\mathcal{N}_0}}\right) = Q\left(|h^n|\, \overline{\mathrm{SNR}^n}\right) \tag{18}$$

where for both monostatic and bistatic cases, $\overline{\mathrm{SNR}^n}$ is defined as:

$$\overline{\mathrm{SNR}^n} = \sqrt{\frac{P^n T}{\mathcal{N}_0}}, \quad n \in U, \tag{19}$$

where P^n is defined in Eqs. (13) and (9), for monostatic and bistatic cases, respectively. Eqs. (16), (19) are used below to show that the diversity order of the bistatic architecture is better than that in monostatic systems.

A. Bistatic Case

In the bistatic case the wireless channels are independent and were defined in Eq. (3) and Eq. (10). Thus, we define the random variable $a^n \triangleq |h^n| = a_{\mathrm{CT}}^n\ a_{\mathrm{TR}}^n$. The probability of error of the bistatic system, with the use of the Chernoff bound, is upper bounded by:

$$\begin{aligned} \Pr(e \mid a^n) &= Q\left(a^n \sqrt{\overline{\mathrm{SNR}^n}}\right) \\ &\le \frac{1}{2}\ \exp\left\{-\frac{(a^n)^2\ \overline{\mathrm{SNR}^n}}{2}\right\} \\ &= \frac{1}{2}\exp\left\{-\frac{\left(a_{\mathrm{CT}}^n\right)^2 \left(a_{\mathrm{TR}}^n\right)^2 \overline{\mathrm{SNR}^n}}{2}\right\}. \end{aligned} \tag{20}$$

It can be shown [11, Eq. (62)]:

$$\begin{aligned} \Pr(e \,|\, \mathrm{tag}\ n) &= \mathop{\mathbb{E}}_{a^n}\left[\Pr(e \mid a^n)\right] = \mathop{\mathbb{E}}_{a_{\mathrm{CT}}^n\ a_{\mathrm{TR}}^n}\left[\Pr(e \mid a_{\mathrm{CT}}^n, a_{\mathrm{TR}}^n)\right] \\ &\overset{(20)}{\le} \left(\frac{2}{\overline{\overline{\mathrm{SNR}^n}}}\right) \exp\left\{\frac{2}{\overline{\overline{\mathrm{SNR}^n}}}\right\} \Gamma\left(0, \frac{2}{\overline{\overline{\mathrm{SNR}^n}}}\right), \end{aligned} \tag{21}$$

where $\Gamma(a, x)$ is the incomplete gamma function, defined as: $\Gamma(a, x) = \int_x^\infty t^{a-1}\ e^{-t} dt$.

After some calculations it can be shown that $\forall n \in U$ the order of decay of the probability of error is [11, Eq. (64)]:

$$\lim_{\overline{\mathrm{SNR}^n} \to \infty} \frac{\log\left[\left(\frac{2}{\overline{\overline{\mathrm{SNR}^n}}}\right) \exp\left\{\frac{2}{\overline{\overline{\mathrm{SNR}^n}}}\right\} \Gamma\left(0, \frac{2}{\overline{\overline{\mathrm{SNR}^n}}}\right)\right]}{\log\ \overline{\overline{\mathrm{SNR}^n}}} = -1. \tag{22}$$

Since the bit error probability upper bound decays with $\frac{1}{\overline{\overline{\mathrm{SNR}^n}}}$, the diversity order of the bistatic system is at least 1.

B. Monostatic Case

In the monostatic case the wireless channels are fully correlated and were defined in Eq. (3) and Eq. (14). Thus, we define the random variable $a^n \triangleq |h^n| = a_{\mathrm{TR}}^2$, which follows exponential distribution with $\mathbb{E}[a^n] = 1$.

The probability of error of the monostatic system is given by:

$$\begin{aligned}\Pr\left(e\,|\,\text{tag } n\right) &= \underset{a^n}{\mathbb{E}}\left[\Pr\left(e \mid a^n\right)\right] = \int_0^\infty Q\left(x\sqrt{\overline{\text{SNR}^n}}\right)e^{-x}dx \\ &= \frac{1}{2} - \exp\left\{\frac{1}{2\,\overline{\text{SNR}^n}}\right\}Q\left(\frac{1}{\sqrt{\overline{\text{SNR}^n}}}\right) \end{aligned} \quad (23)$$

After some calculations, it can be shown that the order of decay [18] of the error probability is:

$$\lim_{\overline{\text{SNR}^n}\to\infty} \frac{\log\left[\Pr(e \mid \text{tag } n)\right]}{\log\ \overline{\text{SNR}^n}} = -\frac{1}{2}, \quad n \in U. \quad (24)$$

From Eq. (24) it can be deduced that the probability of bit error for each tag $n \in U$ decays with $\frac{1}{\sqrt{\overline{\text{SNR}^n}}}$ and hence, the diversity order of the monostatic link is $\frac{1}{2}$.

IV. Probability of Outage

A. Monostatic Case

The signal-to-interference-plus-noise ratio (SINR) of tag n for the monostatic topology is defined as:

$$\text{SINR}^n \triangleq \frac{\frac{1}{R}g_n P^n}{\frac{1}{R}\sum_{j\in\mathcal{A}(n)} P^j g^j s_{nj} + \mathcal{N}_0}, \quad n \in U \quad (25)$$

where $\mathcal{A}(n)$ is the set of tags with adjacent frequencies with respect to tag n, with $|\mathcal{A}(n)| \in \{1,2\}$. $|\mathcal{A}(n)| = 2$ when tag n uses intermediate frequencies with respect to the total available sub-carrier frequencies or equals to 1, otherwise. This is because each tag operates on different sub-carrier frequency and interference is caused only by tags operating on neighboring (i.e. adjacent) sub-carrier frequencies. P^n is defined in Eq. (13), $\mathcal{N}_0$ is the noise power spectral density (Watt/Hz) at the receiver, $R \cong \frac{1}{T}$ is the bit-rate of the tag, and $g_n = |h^n|^2$ is the square of an exponential random variable with $\mathbb{E}\left[|h^n|\right] = 1$.

Parameter s_{nj} is inversely proportional to the sub-carrier frequency separation between tag n and tag j. It depends on the spectral efficiency of the specific binary modulation implemented on each tag and the filtering functions at the reader (assuming equal spacing between $\{F_0^n\}_{n\in U}$ and $\{F_1^n\}_{n\in U}$):

$$s_{nj} = m^{-\nu}\left|F_i^n - F_i^j\right|^{-\nu}, \quad i \in \mathbb{B},\ j \in \mathcal{A}(n). \quad (26)$$

For BFSK modulation, $\nu = 2$ and $m = 2\pi/R$.

In order to calculate the probability of outage of tag n, we need to calculate the PDF of g_n. Since the compound channel $|h^n|$ is exponentially distributed, g_n's PDF is given by [19, pp. 199]:

$$f_{g^n}(x) = \frac{1}{2\sqrt{x}}e^{-\sqrt{x}}, \quad x \geq 0 \quad (27)$$

and its cumulative distribution function (CDF) [19, pp. 199]:

$$F_{g^n}(x) = \int_0^x f_{g^n}(y)\,dy = 1 - e^{-\sqrt{x}}, \quad x \geq 0. \quad (28)$$

The outage event, $\text{SINR}^n \leq \Theta$, occurs when the SINR for the tag-of-interest n drops below a predetermined threshold Θ, necessary for detection at the receiver. The outage probability:

$$\begin{aligned}\Pr_{\text{out}} &= \Pr\{\text{SINR}^n \leq \Theta\} \\ &= \Pr\left(g^n \leq \frac{\Theta R\mathcal{N}_0}{P^n} + \frac{\Theta}{P^n}\sum_{j\in\mathcal{A}(n)} s_{nj}g^j P^j\right) \quad (29) \\ &\overset{(a)}{=} \underset{\text{I}}{\mathbb{E}}\left[F_{g^n}\left(\frac{\Theta R\mathcal{N}_0}{P^n} + \frac{\Theta \text{I}}{P^n}\right)\middle|\,\text{I}\right] \\ &= \underset{\text{I}}{\mathbb{E}}\left[1 - \exp\left\{-\left(\frac{\Theta\text{I}}{P^n} + \frac{\Theta R\mathcal{N}_0}{P^n}\right)^{\frac{1}{2}}\right\}\middle|\,\text{I}\right], \quad (30)\end{aligned}$$

where in (a) we utilized the law of iterated expectation and I is the total interference, i.e., $\text{I} = \sum_{j\in\mathcal{A}(n)} s_{nj}g^j P^j$.

It can be proved that the CDF is a concave function, hence by using the Jensen inequality, in order to avoid the calculation of Eq. (30), we set:

$$\begin{aligned}\Pr_{\text{out}} &\leq 1 - \exp\left\{-\left(\frac{\Theta\mathbb{E}\left[\text{I}\right]}{P^n} + \frac{\Theta R\mathcal{N}_0}{P^n}\right)^{\frac{1}{2}}\right\} \\ &= 1 - \exp\left\{-\left(\frac{2\Theta\text{A} + \Theta R\mathcal{N}_0}{P^n}\right)^{\frac{1}{2}}\right\}, \quad (31)\end{aligned}$$

where we used the fact that $\mathbb{E}\left[\text{I}\right] = 2\text{A} = 2\sum_{j\in\mathcal{A}(n)} P^j s_{nj}$.

B. Bistatic Case

Similarly to the monostatic case, the SINR of user $n \in U$, for the bistatic topology is defined as:

$$\text{SINR}^n \triangleq \frac{\frac{1}{R}g^n P^n}{\frac{1}{R}\sum_{j\in\mathcal{A}(n)} P^j g^j s_{nj} + \mathcal{N}_0}, \quad n \in U \quad (32)$$

where $g^n = |h_{\text{CT}}^n h_{\text{TR}}^n|^2$ is the square of the product of two independent Rayleigh-distributed random variables. We set again I the total interference, i.e., $\text{I} = \sum_{j\in\mathcal{A}(n)} s_{nj}g^j P^j$. Let a^n the random variable following the product of two Rayleigh distributed random variables, a_{CT}^n and a_{TR}^n. The PDF of a^n is given by [19, pp. 302] [20, pp. 370, Eq. 2.478.4]:

$$\begin{aligned}f_{a^n}(x) &= \int_0^{+\infty} \frac{1}{y} f_{a_{\text{CT}}^n}(y) f_{a_{\text{TR}}^n}\left(\frac{x}{y}\right)dy \\ &= 4x\int_0^{+\infty}\frac{1}{y}\exp\left\{-y^2 - \frac{x^2}{y^2}\right\}dy \\ &= 4x\text{K}_0(2x), \quad x \geq 0, \quad (33)\end{aligned}$$

where K_0 is the zero-order modified Bessel function of the second kind. The PDF of $g^n = (a^n)^2$ is given by [19, pp. 199]:

$$f_{g^n}(x) = 2\text{K}_0\left(2\sqrt{x}\right), \quad x \geq 0, \quad (34)$$

and the CDF is:

$$F_{g^n}(x) = \int_0^x f_{g^n}(y)\,dy = 1 - 2\sqrt{x}\text{K}_1\left(2\sqrt{x}\right), \ x \geq 0, \quad (35)$$

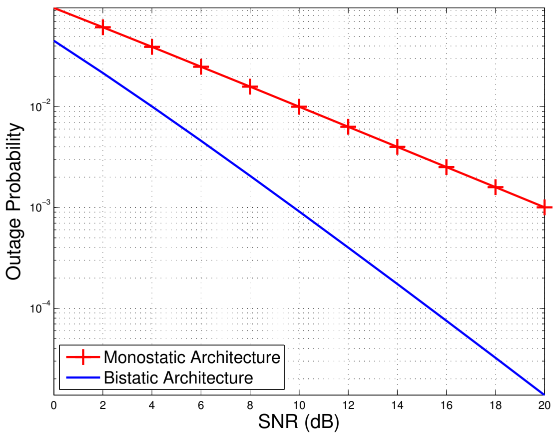

Fig. 2. The outage probability of the monostatic and the bistatic architectures, without interferers, for Θ corresponding to $\mathrm{SNR} = 10$ dB.

where K_1 is the first-order modified Bessel function of the second kind. Again, we calculate the probability of outage:

$$\begin{aligned}\mathrm{Pr}_{\mathrm{out}} &= \mathrm{Pr}\left(\mathrm{SINR}^n \leq \Theta\right) = \mathrm{Pr}\left(g^n \leq \frac{\Theta \mathrm{I}}{P^n} + \frac{\Theta R \mathcal{N}_0}{P^n}\right) \\ &= \mathop{\mathbb{E}}_{\mathrm{I}}\left[F_{g^n}\left(\frac{\Theta \mathrm{I}}{P^n} + \frac{\Theta R \mathcal{N}_0}{P^n}\right)\middle| \mathrm{I}\right] \\ &= \mathop{\mathbb{E}}_{\mathrm{I}}\left[1 - 2H(\mathrm{I})\mathrm{K}_1\left(2H(\mathrm{I})\right)|\mathrm{I}\right], \end{aligned} \tag{36}$$

where $H(\mathrm{I}) = \left(\frac{\Theta \mathrm{I}}{P^n} + \frac{\Theta R \mathcal{N}_0}{P^n}\right)^{\frac{1}{2}}$. It can be shown that the CDF is concave. Therefore, by using the Jensen inequality we get:

$$\mathrm{Pr}_{\mathrm{out}} \leq 1 - 2\left(\frac{\Theta \mathrm{A} + \Theta R \mathcal{N}_0}{P^n}\right)^{\frac{1}{2}} \mathrm{K}_1\left(2\left(\frac{\Theta \mathrm{A} + \Theta R \mathcal{N}_0}{P^n}\right)^{\frac{1}{2}}\right) \tag{37}$$

where we used the fact that $\mathbb{E}\left[\mathrm{I}\right] = \mathrm{A} = \sum_{j \in \mathcal{A}(n)} P^j s_{nj}$.

V. Numerical Results

Taking into account that for each tag only two interferers exist, several network topologies with three tags (the tag-of-interest and two interferers) were simulated. The parameters used in the simulations are shown at Table I. In all tested topologies the reader is placed at the middle of the test area, which is an 100×100 m^2 grid, with 1 m resolution. In order to determine threshold Θ, we fix the outage probability of the monostatic architecture to 1% and work without interferers. Therefore Θ is calculated as follows using (19) and (30):

$$\begin{aligned}&\mathrm{Pr}_{\mathrm{out}}(\mathrm{SNR}^n \leq \Theta) = F_{g^n}\left(\frac{\Theta R \mathcal{N}_0}{P^n}\right) = F_{g^n}\left(\frac{\Theta}{\mathrm{SNR}^2}\right) \Rightarrow \\ &\Rightarrow F_{g^n}\left(\frac{\Theta}{\mathrm{SNR}^2}\right) = y \Rightarrow F_{g^n}^{-1}(y) = \frac{\Theta}{\mathrm{SNR}^2}\end{aligned} \tag{38}$$

We calculate the inverse of (28):

$$F_{g^n}^{-1}(y) = \ln^2(1 - y), \tag{39}$$

TABLE I
PARAMETERS FOR NUMERICAL RESULTS

$G_{\mathrm{Tx}} = G_{\mathrm{Rx}} = 2.15$ dBi	$h_{\mathrm{T}} = 2$ m	$\lambda = \frac{1}{3}$ m
$R = 1$ Kbps	$h_{\mathrm{R}} = 2$ m	
$\eta = -10$ dB	$h_{\mathrm{C}} = 2$ m	

and substitute in Eq. (38) in order to get outage probability of 1%:

$$\ln^2(1 - 1\%) = \frac{\Theta}{\mathrm{SNR}^2} \Rightarrow \Theta = \mathrm{SNR}^2 \ln^2(0.99) \tag{40}$$

For example, for given $\mathrm{SNR} = 20$ dB, we calculate the parameter $\Theta \approx 1$. In Fig. 2 the probability of outage without interferers, for Θ corresponding to $\mathrm{SNR} = 10$ dB is depicted (the same Θ is used thereinafter). Literally, this figure shows the probability of deep fade in the two architectures and it can be deduced that the monostatic architecture has two orders of magnitude bigger probability of deep fade than the bistatic architecture.

In Fig. 3 the first setup is depicted; the distances between the components are small and thus, the probability of outage is small, as shown in Fig. 4. The bistatic architecture achieves better performance, even better than the desired 1% at 10 dB SNR. Moreover, in setup 2, shown in Fig. 5, the emitter is placed at one corner of the test area and the interfering tags are placed between the reader and the emitter, while the tag-of-interest is placed further away from the emitter. This topology favors the monostatic architecture because the distance between the reader and the tag is much smaller than the distance between the tag and the emitter. From Fig. 6 can be deduced that the bistatic architecture has better performance than the monostatic one, even though the performance gap closes due to the large distance between the carrier emitter and the tag-of-interest. In the final scenario, the emitter is placed at the edge of the field and the tag-of-interest at the opposite edge, thus the emitter-to-tag distance is maximized. The two interferers are placed in-between the emitter and the reader, as shown in Fig. 7. One could expect that the monostatic architecture would have better performance, but the results of Fig. 8 suggest otherwise. Again the bistatic architecture has better probability of outage than the monostatic. In this case the derived bounds are not as exact as in the other two scenarios, since the tag-of-interest-to-emitter distance is large and the interference is strong. It is clear that the bistatic architecture offers improved coverage and performance, in contrast to the monostatic one.

VI. Implementing a Scatter Sensor Network Using the Bistatic Architecture

A. Network Architecture

From both the single user and the multi-user analysis, it can be deduced that the bistatic architecture guarantees better performance and coverage. Thus, to create dense scatter sensor networks, the bistatic architecture should be utilized. Using this fact, a digital scatter sensor network of maximum

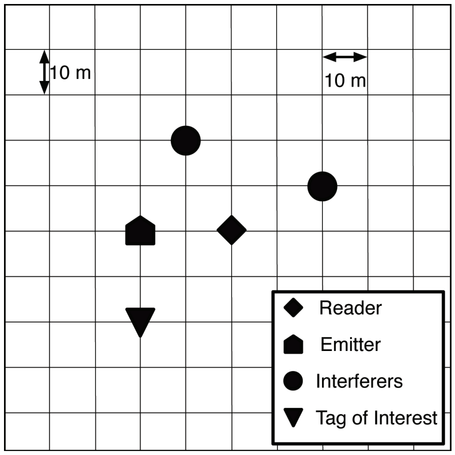

Fig. 3. Simulation setup 1. The tags and the emitter are close to the reader, resulting to good performance for both architectures.

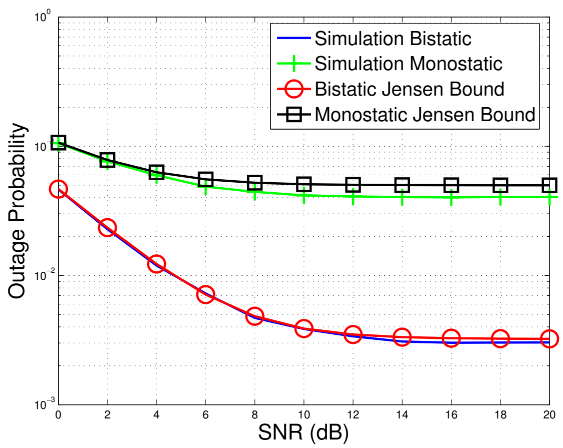

Fig. 4. Probability of outage of monostatic and bistatic systems and the corresponding Jensen Bounds for setup 1.

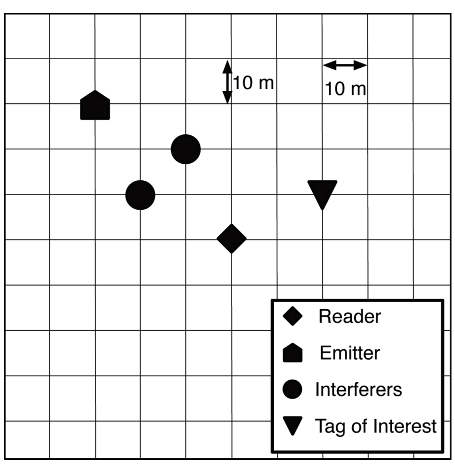

Fig. 5. Simulation setup 2. The emitter is placed on the edge of the field and the tag-of-interest is moved away from the emitter, while the two interferers are closer to the emitter and the reader.

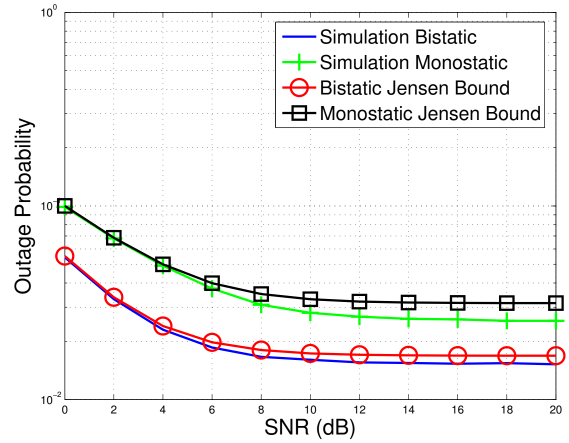

Fig. 6. Probability of outage of monostatic and bistatic systems and the corresponding Jensen Bounds for setup 2.

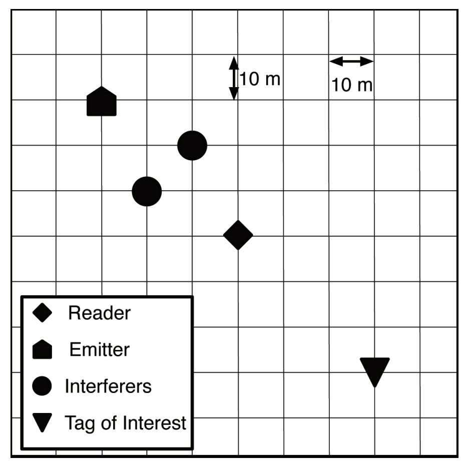

Fig. 7. Simulation setup 3. The distance between the emitter and the tag-of-interest is almost maximum.

45 tags, in each cell, is proposed. The network consists of prototype digital scatter tags, multiple carrier emitters and a single SDR receiver. The proposed network is designed for agricultural applications and thus low-cost and low-power nodes are needed. Moreover, sensed data e.g. air humidity, temperature and soil moisture, change slowly with time, thus low bit rate (1 Kbps) is appropriate.

The prototype tags consist of a micro-controller unit (MCU), a RF transistor and a crystal oscillator used for the MCU clocking. In order to keep the tag cost as low as possible, the MCU is responsible for the physical layer communication (through reflection), as well as sensing. The MCU gathers data from the analog-to-digital converter (ADC), uses a simple Reed-Muller encoding [12] for channel coding and transmits the encoded data with BFSK modulation. Since the tags implement BFSK modulation, two frequencies must be generated by each MCU. The ability of the MCU to produce a number of different frequency pairs, facilitates the use of FDM for multi-user communication. But the lack of PLLs or external

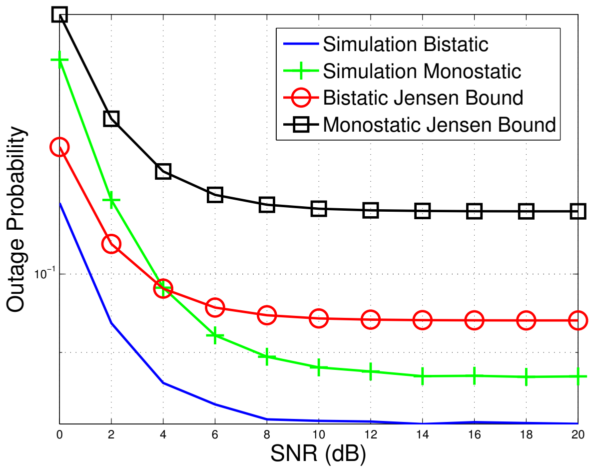

Fig. 8. Probability of outage of monostatic and bistatic systems and the corresponding Jensen Bounds for setup 3. The network components are far away (bistatic architecture) and the performance is expected to decrease. Instead, the bistatic has better performance than the monostatic.

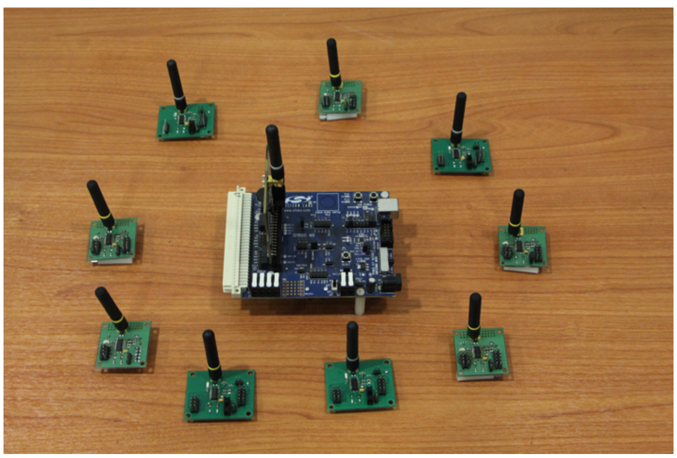

Fig. 9. Backscatter cell example: 8 tags and an emitter.

components for frequency generation creates many challenges, which limit the capacity of the network and are described in the next section.

In order to create a dense scatter sensor network, cellular architecture must be used, where each cell contains a carrier emitter surrounded by several scatter tags (Fig. 9). The carrier emitters are low cost embedded radios operating at the 868 MHz band (European ISM band), transmitting at maximum 13 dBm. The cells are placed around the *single* reader, which is responsible for the reception and decoding of the tags. Time division multiple-access (TDMA) protocol is used by the carrier emitters in order to ensure that only one cell is active at each time frame. In a single time frame, the carrier emitter transmits the carrier signal and the tags transmit their information to the reader.

Each user has a guard band surrounding its transmitting frequencies ($W_{\mathrm{G}} = 500$ Hz) in order to ensure that the environmental changes (i.e., frequency and humidity changes) will not cause aliasing between the adjacent users.

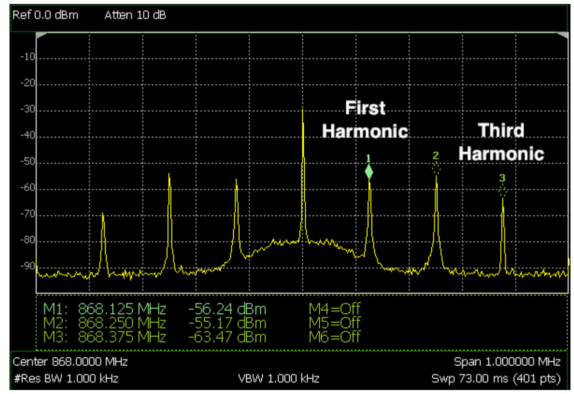

Fig. 10. Spectrum of a single tag transmitting BFSK modulation, as well as the third harmonic of F_0.

B. Implementation Constraints

The specific, implemented use of the MCU for the frequency generation and modulation, reduces the network capacity. The MCU has a system clock operating at maximum $F_s = 24.5$ MHz and a software frequency divider creates the frequency pairs. This means that the produced frequencies are sub-multiples of the system clock frequency. The function connecting the system clock and the output frequency is not linear. This limits the maximum number of frequencies produced and challenges the satisfaction of the necessary orthogonality criteria presented in Eq. (5).

Moreover, an inherent constraint exists in the specific FSK implementation. The 50% duty cycle of the produced periodic waveforms (with different subcarrier frequency for each bit) [10] results to the appearance of the signal's third harmonic, as shown in Fig. 10. This results to the limitation of the system's total available bandwidth.

The proposed network operates on the frequency range from 100 to 300 KHz around 868 MHz, with total bandwidth $W =$ 200 KHz. The available bandwidth can be distributed over $N = 45$ users, each operating on different pairs of frequencies $\pm F_i^n, i \in \mathbb{B}$ and $n \in U$. In Fig. 11 the spectrum of five users transmitting simultaneously is depicted. Each tag can gather data from the ADC, encode them and transmit them to the SDR receiver. The range of the prototype tags is more than 150 m [10], [12] and this is more than enough to have full coverage of an average agricultural field.

VII. Conclusion

This work presented an in-depth analysis of the system models for both monostatic and bistatic architectures of scatter WSNs. Closed form expressions for the probability of error under ML detection and the diversity order for the single user case are developed. Jensen bounds of probability of outage for multiple user case were also derived. It was shown that the bistatic architecture surpasses the monostatic in terms of coverage and performance and it should be used in order to

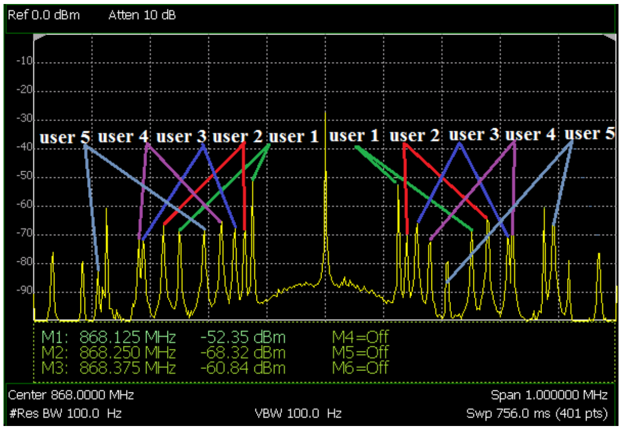

Fig. 11. Five users spectrum.

construct dense scatter WSNs. Finally, a prototype bistatic digital scatter network using FSK modulation and FDM, with maximum 45 nodes was presented.

Acknowledgments

This work was supported by the ERC-04-BLASE project, executed in the context of the ”Education & Lifelong Learning” Operational Program of the National Strategic Reference Framework (NSRF), General Secretariat for Research & Technology (GSRT), funded through European Union-European Social Fund and Greek national funds.

References

[1] H. Stockman, “Communication by means of reflected power,” *Proc. IRE*, pp. 1196–1204, 1948.

[2] K. Finkenzeller, *RFID Handbook: Fundamentals and Applications in Contactless Smart Cards and Identification*, 2nd ed. New York, NY: John Wiley and Sons, 2003.

[3] J. Paradiso, L. Pardue, K. Hsiao, and A. Benbasat, “Electromagnetic tagging for electronic music interfaces,” in *Journal of New Music Research*, vol. 32, Dec. 2003, pp. 395–409.

[4] J. Paradiso, K. Hsiao, and A. Benbasat, “Tangible music interfaces using passive magnetic tags,” in *ACM Conf. Human Factors in Computing Systems: Special Workshop on New Interfaces for Musical Expression*, Chicago, IL, 2001.

[5] *EPC Radio-Frequency Identity Protocols, Class-1 Generation-2 UHF RFID Protocaol for Communications at 860 MHZ-960 MHZ.* EPC Global, 2008, version 1.2.0.

[6] G. Vannucci, A. Bletsas, and D. Leigh, “A software-defined radio system for backscatter sensor networks,” *IEEE Trans. Wireless Commun.*, vol. 7, no. 6, pp. 2170–2179, Jun. 2008.

[7] A. P. Sample, D. J. Yeager, and J. R. Smith, “Design of a passively-powered, programmable sensing platform for UHF RFID systems,” in *Proc. IEEE Int. Conf. on RFID*, Grapevine, TX, Mar. 2007.

[8] C. M. Kruesi, R. Vyas, and M. Tetzeris, “Design and development of a novel 3D cubic antenna for wireless sensor networks (WSN) and RFID applications,” *IEEE Trans. Antennas Propag.*, vol. 57, no. 10, pp. 3293 – 3299, Oct. 2009.

[9] V. Lakafosis, A. Rida, Y. Li, S. Nikolaou, and M. M. Tenteris, “Progress towards the first wireless sensor networks consisting of inkjet-printed, paper-based RFID-enabled sensor tags,” *Proc. IEEE*, vol. 98, pp. 1601–1609, Sep. 2010.

[10] J. Kimionis, A. Bletsas, and J. N. Sahalos, “Increased range bistatic scatter radio,” *IEEE Trans. Commun.*, vol. 62, no. 3, pp. 1091–1104, Mar. 2014.

[11] N. Fasarakis-Hilliard, P. N. Alevizos, and A. Bletsas, “Coherent detection and channel coding for bistatic scatter radio sensor networking,” *IEEE Trans. Commun.*, vol. 63, pp. 1798–1810, May 2015.

[12] P. N. Alevizos, N. Fasarakis-Hilliard, K. Tountas, N. Agadakos, N. Kargas, and A. Bletsas, “Channel coding for increased range bistatic backscatter radio: Experimental results,” in *Proc. IEEE RFID Techn. and Applications (RFID-TA)*, Tampere, Finland, Sep. 2014, pp. 38–43.

[13] P. N. Alevizos and A. Bletsas, “Noncoherent composite hypothesis testing receivers for extended range bistatic scatter radio WSNs,” in *Proc. IEEE Int. Conf. on Commun. (ICC)*, London, U.K., Jun. 2015.

[14] J. Griffin and G. Durgin, “Complete link budgets for backscatter-radio and RFID systems,” *IEEE Antennas Propag. Mag.*, vol. 51, no. 2, pp. 11–25, Apr. 2009.

[15] J. Griffin and G. D. Durgin, “Link envelope correlation in the backscatter channel,” *IEEE Commun. Lett.*, vol. 11, no. 9, pp. 735 –737, Sep. 2007.

[16] A. Bletsas, S. Siachalou, and J. N. Sahalos, “Anti-collision backscatter sensor networks,” *IEEE Trans. Commun.*, vol. 8, no. 10, pp. 5018 – 5029, Oct. 2009.

[17] E. Kampianakis, J. Kimionis, K. Tountas, C. Konstantopoulos, E. Koutroulis, and A. Bletsas, “Wireless environmental sensor networking with analog scatter radio & timer principles,” *IEEE Sensors J.*, vol. 14, no. 10, pp. 3365–3376, Oct. 2014.

[18] D. Tse and P. Viswanath, *Fundamentals of Wireless Communication*. New York, NY: Cambridge University Press, 2005.

[19] A. Pappoulis and S. U. Pillai, *Probability, Random Variables and Stochastic Processes*, 4th ed. New York, NY: McGraw-Hill, 2002.

[20] A. Jeffrey and D. Zwillinger, *Table of Integrals, Series, and Products*, 7th ed. Elsevier/Academic Press, Amsterdam, 2007.